Solid State Phenomena
ISSN: 1662-9779, Vol. 389, pp 227-241
doi:10.4028/p-k4HkEk

Submitted: 2026-01-19
Revised: 2026-02-17
Accepted: 2026-02-24
Online: 2026-04-16

Rubber Forming as a Novel Manufacturing Approach for Bipolar Plates in Fuel Cell Systems

Bernd-Arno Behrens[1,a], Sven Hübner[1,b], Simon Pauli[2,c], Henner Rüschkamp[2,d], Simon Kimmina[1,e], Denis Fink[1,f], Behdad Yaalimadad[1,g*]

[1]Leibniz University Hanover, Institute of Forming Technology and Machines, An der Universität 2, 30823 Garbsen, Germany

[2]Aspens GmbH, Feodor-Lynen-Straße 27, 30625 Hanover, Germany

[a]behrens@ifum.uni-hannover.de, [b]huebner@ifum.uni-hannover.de, [c]s.pauli@aspens.de, [d]h.rueschkamp@aspens.de, [e]s.kimmina@stud.uni-hannover.de, [f]fink@ifum.uni-hannover.de, [g*]yaalimadad@ifum.uni-hannover.de

Keywords: fuel cell systems, bipolar plates, sheet metal forming, rubber forming.

Abstract. Hydrogen-based energy systems are considered a key pillar of the energy transition, yet the cost-efficient, mass production of metallic bipolar plates (BPPs) for proton exchange membrane fuel cells (PEMFCs) remains challenging, as conventional processes are limited by comparatively long cycle times and forming-related instabilities. This paper investigates the rubber drawing process as a cost-efficient manufacturing method for metallic bipolar plates, proposed as an alternative to the commonly applied hydroforming process, analysing the influence of pressing force, rubber hardness and thickness, tool modifications for varying pressure distribution, and the suitability of additively manufactured tool dies made from Maraging Steel 1 (X3NiCoMoTi 18-9-5) or ceramic-filled UV resin. The results show that precise and stable tool guidance, as well as a well-adapted tool setup, are required to achieve reproducible component quality; targeted adjustments of process and rubber parameters improved channel dimensional accuracy, but revealed limited forming capability in certain areas. Furthermore, concavely and convexly modified rubber dies reduced component warping in specific directions, and steel dies exhibited higher precision and less distortion compared to ceramic-filled UV resin dies. These findings highlight the potential of the rubber drawing process for cost-effective production of bipolar plates, while identifying key parameters for further optimization toward industrial-scale manufacturing.

Introduction

Fuel cells are considered a key technology for sustainable mobility and a promising option for reducing emissions in the transport sector. Compared to conventional internal combustion engines, fuel cell systems enable locally emission-free operation and higher overall energy efficiency. In addition to battery electric vehicles, hydrogen-based mobility concepts offer advantages such as high energy density and short refueling times, making them particularly suitable for applications with extended range requirements [1, 2]. A widely used fuel cell technology is the proton exchange membrane fuel cell (PEMFC). In PEMFCs, electrical energy is generated through the electrochemical reaction of hydrogen and oxygen to form water, ensuring a continuous on-board power supply in fuel cell electric vehicles (FCEVs). This addresses key limitations of pure electromobility, including limited driving range and long charging times, while maintaining high system efficiency [1, 2]. Fig. 1 illustrates the exemplary structure of a fuel cell stack composed of multiple individual cells connected in series to achieve a nominal voltage of approximately 400 V. Each single cell comprises a membrane electrode assembly (MEA), which consists of a catalyst-coated membrane and adjacent gas diffusion layers, as well as bipolar half plates that enable reactant distribution and electrical conduction. Together with the current collectors, these components facilitate the electrochemical conversion of hydrogen and oxygen into electrical energy [3, 19]. The individual cells are stacked in

series and electrically interconnected, while the entire fuel cell stack is mechanically clamped and electrically contacted by current collectors and end plates, as shown in Fig. 1 [19].

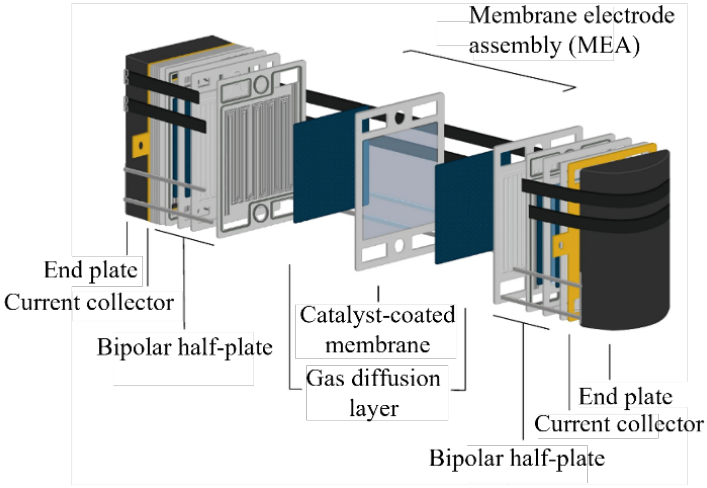

Fig. 1. Fuel cell stack [19].

The bipolar plate (BPP), consisting of two monopolar plates (MPP), is a central structural component of the cell. It performs essential functions such as charge transport, gas supply, removal of reaction products, cooling, and separation of media [4]. These diverse tasks place high demands on corrosion resistance, electrical conductivity, and dimensional accuracy. At the same time, BPPs account for about 80 % of the stack weight and 45 % of the stack costs [5]. The high costs result primarily from the complex manufacturing processes, which require high precision due to the intricate microchannel structures of bipolar plates. Fig. 2 shows a cross-sectional view of a BPP, illustrating the characteristic channel geometry from a side perspective and highlighting the stringent geometric requirements involved (dimensions in mm) [6, 20]. Conventional processes such as hollow stamping reach their limits when it comes to complex channel geometries and thin-walled materials. Alternative forming processes such as hydroforming can provide improved dimensional accuracy and surface quality for metallic bipolar plates. However, the process is characterized by long cycle times due to the need for pressure build-up, controlled fluid flow, and pressure holding phases, which significantly limits productivity in high-volume manufacturing [7]. In addition, the requirement for high-pressure-capable tooling and sealing systems results in elevated tool complexity and costs, making hydroforming economically unattractive for large-scale production [7]. Therefore, intensive research is being conducted into alternative manufacturing technologies, including continuous hollow spinning or roll spinning, which offer high automation potential [1, 8]. Although these processes enable high production rates (up to 120 MPP/min), they have limitations in terms of flexibility and component homogeneity [9].

Rubber pad forming is a particularly promising alternative, as it employs a highly compliant, entropically elastic medium instead of a geometrically rigid metallic die. This enables a more uniform and adaptive pressure distribution, allowing gentle and flexible forming of sensitive surfaces. Originally known from the aviation industry, the process was developed specifically for large sheet metal components and prototypes [2, 10]. Due to the simple tool design (no sealing of the pressure medium required) and the potentially shorter cycle times, it offers cost advantages over processes such as hydroforming [11]. In addition, the elastic pressure distribution is expected to reduce material thinning and improve surface quality – a decisive advantage for coated or polished materials [12].

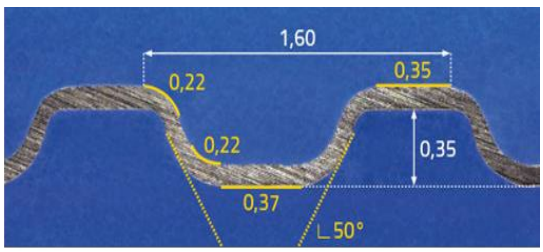

Fig. 2. MPP channel geometry [20].

In recent years, an increasing number of scientific papers have been published on the application of the rubber stamping process to the manufacture of metallic

bipolar plates. Elyasi et al. (2017) investigated the production of stainless steel BPPs using semi-stamp rubber forming and demonstrated a significant improvement in the fill ratio (+11.7 %), thickness distribution, and dimensional accuracy compared to conventional rubber pad forming [13]. Hashemi and Roohi (2021) evaluated the influence of process parameters such as rubber hardness, pressing force, and stamp speed on aluminum BPP with helical channels and identified a Shore A hardness of 60 as optimal for maximum channel depth [14]. Elyasi et al. (2016) additionally showed that the design of the tool gap (the so-called “die clearance”) significantly influences the dimensional accuracy and service life of the rubber die [15]. More recent work, such as that by Albers and Ngondji (2025), combines rubber pad forming with stampinging technologies (“hybrid forming”) and demonstrates an increase in process accuracy while reducing tool complexity [16].

Furthermore, recent studies indicate that the nonlinear pressure behavior of the elastic medium in the rubber stretching process can lead to local mold instabilities, especially in thin-walled sheets. Groche et al. (2014) identified uneven pressure distributions as the cause of elastic springback and local warping [17], while Kim and Kim (2018) confirmed that the hardness and pressure curve of the elastomer are decisive for the flatness and dimensional accuracy of the components [18]. However, a targeted examination of these instabilities - in particular the so called 'snap-through' effect - in the manufacture of metallic bipolar plates has not yet been carried out, which underlines the existing research gap and the relevance of the present work.

This work deals with the investigation of the dimensional and shape accuracy of metallic bipolar plates (BPP) in the rubber drawing process as a function of various process parameters. The focus is on analyzing the influences of pressing force, holding time, rubber hardness, and rubber thickness on the resulting component geometry as well as on local shape instabilities such as warping and the 'snap-through' effect. Geometric features such as draw depth, edge sharpness, flatness, and reproducibility of the channel structures were evaluated. In addition, the occurrence of elastic springback and local deformations was investigated in order to identify correlations between pressure distribution, material properties of the rubber, and component distortion.

Various tool materials were used to carry out the tests, including ceramic-filled UV-cured resin (CR) and Maraging Steel 1 (MS1), each of which was additively manufactured. The manufacturability of additively manufactured matrices, like those depicted (CR and steel), and their suitability for the production process in terms of feasibility were evaluated. Furthermore, the reproducibility and cost-effectiveness of the process were also evaluated. In addition, the test and tool setup was specifically modified, e.g., by using convex and concave steel masks placed on the rubber pad (Fig. 4). These modifications influence the local pressure distribution during the forming process and its development over time in the course of the process. The aim was to analyse the influence of this coupled spatial-temporal pressure distribution on the flatness of the components, as it contributes significantly to the development of nonlinear form instabilities (cf. [17, 18]).

The aim of the investigations is to quantify the influence of these parameters on dimensional accuracy and dimensional stability and to develop strategies for minimizing warping. For the experimental implementation, a simplified channel design and a reduced component size were chosen in order to enable a high number of reproducible test runs with low material consumption.

Materials and Methods

The rubber materials used for the forming experiments were based on polyurethane (PU). Polyurethane sheets and mats were supplied by Fibro GmbH, including thin mats with thickness of 1 mm and hardness of 90 and 95 Shore A, as well as Fibroelast and Fibroflex sheets with thickness of 20 mm and hardnesses of 65 Shore A (Fibroelast) and 80–95 Shore A (Fibroflex). All rubber materials were cut to a stamp size of 50 × 50 mm, corresponding to the selected demonstrative component geometry. The Fibroelast and Fibroflex plates were also prepared in thicknesses of 5, 10, and 15 mm. The CR dies were manufactured by Aspens through 3D printing and provided for the investigations. After UV-curing, they were additionally heat-treated at 150 °C. The size of each die was 50 x 50 x 10 mm. The CAD geometry shown in Fig. 3 represents a simplified channel design developed by Aspens and used for the investigations. In addition, steel dies with equal size made of MS1

(X3NiCoMoTi 18-9-5), a high-strength, precipitation-hardening steel, were printed by IPEG (Institute for Product Development and Device Engineering) using a powder laser process. The material used to manufacture the MPP was X2CrNiMo17-12-2 (1.4404) austenitic stainless steel. The 0.1 mm thick sheet metal blanks were also cut to a size of 50 × 50 mm.

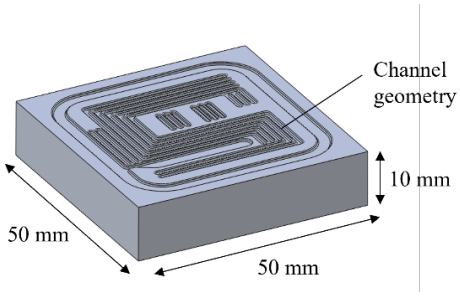

Fig. 3. CAD model of the die with simplified channel geometry.

For the forming experiments a hydraulic press Hydrap HPDZb 63 was used. The system has a CNC press control with a monitor for precise input of process and tool parameters and enables ram forces of 63 – 630 kN, drawing cushion forces of 40 – 400 kN, and stroke speeds of 0 – 410 mm/s. Fig. 4 shows the hydraulic press, along with the corresponding schematic representation of the experimental setup used for the rubber pad forming experiments investigating the influence of rubber hardness, rubber thickness, and pressing force. The schematic illustrates the arrangement of the base plate, draw edge, die, sheet blank, rubber pad, and stamp. On the right-hand side, a modified setup is additionally shown, exemplified by a convex steel mask positioned on top of the rubber pad.

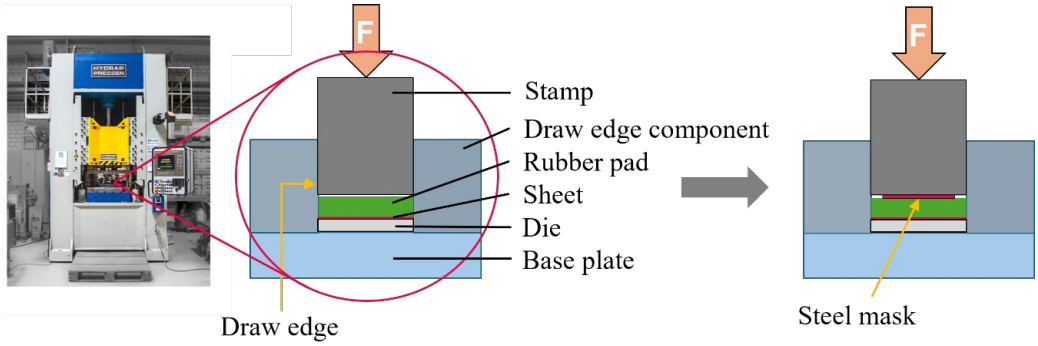

Fig. 4. Schematic representation of the experimental setup without and with mask.

The draw edge tool was manufactured from 1.2740 tool steel based on a CAD model. Fig. 5 shows the CAD representation of the draw edge tool as well as its installation in the hydraulic press, mounted above a load cell with signal amplifier for measuring the actual forming force. The tool consists of a base plate, a bolted draw-edge component, a stamp, and features the dimensions shown in Fig. 5.

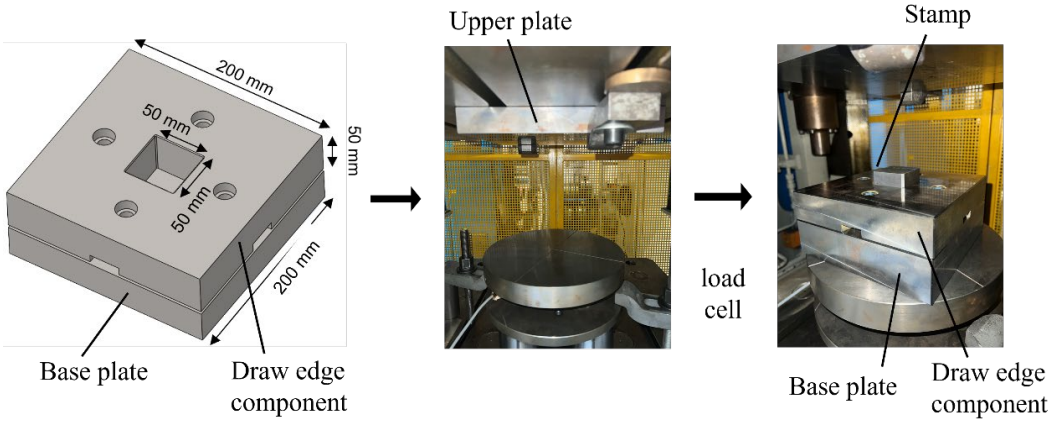

Fig. 5. Draw-edge tool CAD model and installation in the press.

Rubber pads with a hardness of 80 Shore A and a thickness of 10 mm were used to investigate modified concave and convex tool geometries and the resulting force transmission. Concave refers to indentations that are curved inward, while convex describes elevations that are curved outward. These shapes influence the tool geometry and thus the resulting local and temporal pressure distribution during the forming process: Concave areas lead to locally higher pressure and longer contact time,

while convex areas lead to lower pressure and shorter contact time. The elevations were created using steel masks with thicknesses between 1 and 3 mm, which were positioned as shown in Fig 4. They were also produced by milling material out of the rubber pad, resulting in a convex or concave elevation of 2 mm. The planned mask and pad geometries included square, ring-shaped, and grid-like structures are shown in Fig. 6. So far, the square variants have been manufactured and examined; further investigations will address the analysis of ring and grid geometries. Such test parameters that have not yet been carried out are marked with an asterisk (*) in the following figures and tables. The steel mask geometries are shown in their concave configuration. For each geometry, a corresponding negative part remains after removal of the raised structure; this negative directly represents the complementary convex configuration and is likewise used in the experiments.

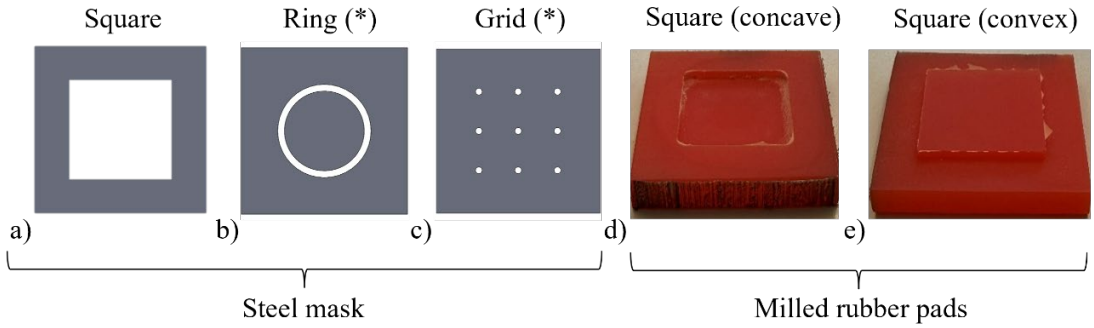

Fig. 6. Representative concave steel mask geometries: (1) square, (2) ring, (3) grid and milled rubber pads: (4) concave (5) convex.

Table 1 provides an overview of the material parameters of the rubber pads, including rubber hardness and thickness, as well as those of the sheet metal blanks and dies. In addition, the investigated process parameters and modifications, such as pressing force, dwell time, and mask geometry, are summarized. Three tests were carried out for each parameter variation in order to assess the reproducibility of the results and identify outliers.

Table 1. Experimental matrix for the parameter study to improve component geometry.

Parameter	**Levels / Variants**			
Rubber hardness [Shore A]	65	80	95	
Rubber thickness [mm]	5	10	15	
Pressing force [kN]	300	400	500	
Dwell time [s]	0		2	
Mask geometry	Convex / Conkave	Square	Ring (*)	Grid (*)
Die material	Ceramic-filled UV-cured		Maraging Steel 1	

The formed MPPs were then indexed and measured using the Keyence VR-3200 3D profilometer. The system works on the principle of fringe projection and enables non-contact, high-resolution surface characterization. With a height measurement accuracy of 3 µm, a width measurement accuracy of 2 µm, and a repeatability of 0.5 µm, it allows precise 2D and 3D measurements at up to 160x digital magnification. Despite the profile meter's anti-reflection settings, these could not be completely eliminated without additional matting. Attempts at matting using airbrush technology showed that this enables reflection-free 3D measurement. However, due to the large number of samples, matting was not used, as the geometry parameters could be reliably evaluated despite the remaining measurement artifacts.

The component geometry was evaluated based on the measured 2D and 3D height profiles. Characteristic values such as channel depth and geometry, surface quality, and component warping were determined and compared. Further data analysis was performed using Microsoft Excel and

creating response surface plots in Minitab. For the quantitative evaluation of the channel geometry and drawing depth, four characteristic reference measurement points (P1 – P4) were defined representing both wide and narrow channels as well as central and outer areas of the component. To determine component warping, four profile lines were defined across the optically measured sheet metal. The profile lines include a vertical line, a horizontal line, and two diagonal lines, where TL - BR stands for top left to bottom right and BL - TR stands for bottom left to top right. Based on these profiles, the height difference between the highest point at the center of the component surface and a reference line connecting the outer corner points at the edge of the forming zone was determined. In this context, a comparison was carried out between the target geometry (steel die), a standard rubber pad with a thickness of 10 mm and a hardness of 80 Shore A, and the modified setup described above featuring convex and concave elevations. The experiments on component warping were conducted exclusively using the steel die to ensure improved reproducibility and comparability.

Results and Discussion

Using the materials and equipment previously described, all experiments were conducted within the framework of parameter studies and subsequently analyzed and evaluated optically. At the beginning of the investigations, the actual geometries of the CR and steel dies were measured using a Keyence light microscope. Fig. 7 shows such an image capture and measurement. From left to right, real photographic images of the CR and steel dies are displayed first. Next, the determined 3D height profile of these dies can be seen. On the right side, the 2D side-height profile of both dies is depicted, which was determined along the vertical blue arrow in the original image. The labels P1 to P4 in the right image are the measurement points selected for the subsequent analysis to evaluate the channel or drawing depth. Qualitatively, it can be observed in both the 3D and 2D height profiles that the steel die possesses distinctly sharper and deeper channels. While the channel depths of the CR die range from 0.219 to 0.374 mm, the steel dies have channel depths between 0.425 and 0.561 mm. From the 3D height profile representation of the entire component, it can also be seen from the color areas that the channel depths of the CR die lie in a similar range, whereas the steel die exhibits clear height differences in certain channel areas. The gradations of the channels in the middle area (green and blue) are desired recesses that are clearly better manufactured in the steel die. The right section of the image also shows that on a micrometer scale, both dies exhibit global unevenness, both in the surface area and in the channel bottoms. However, locally, the CR die has flatter, smoother surfaces compared to the steel die, which tends to have a wavy surface.

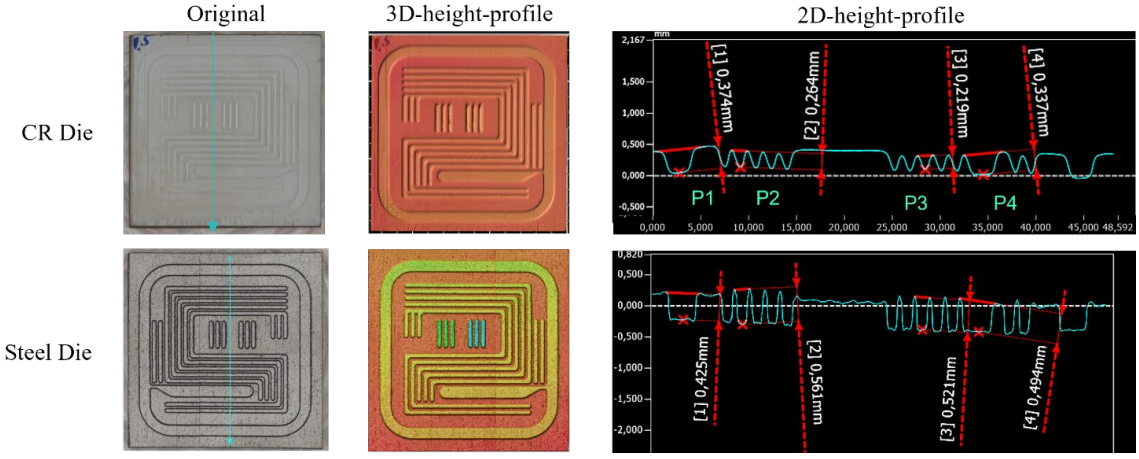

Fig. 7. Optical analysis of the manufactured CR and steel dies.

Fig. 8 presents a detailed comparison of the side profiles from exemplary channel sections (P2) of the two manufactured dies made from CR and steel. This figure highlights the significantly different channel geometries of the CR and steel dies. Apart from channel depths, these differ primarily in their overall geometry. The CR die exhibits a more conical channel geometry with a central low point, whereas the steel die has a more trapezoidal geometry with a flat channel bottom. In comparison with

the target geometry from the state of the art (Fig. 2), it is observed that the steel die features a much better, more precisely manufactured geometry and is closer to the reference geometry from the polished section. Apart from differences in the slope of the edge regions, the channel width at P2 is approximately the same for both dies, while the CR die achieves a channel depth of 0.264 mm and the steel die reaches a channel depth of 0.561 mm. However, the actual channel depths are to be disregarded, and instead, a qualitative assessment of the geometry should be employed, as the CAD geometry (target geometry) used for die fabrication was only constructed in reference to the actual target geometry in order to facilitate representative qualitative executions and evaluations.

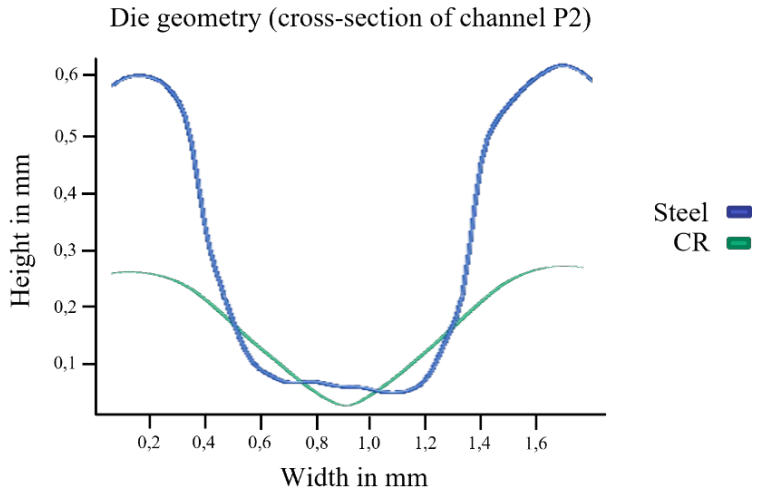

Fig. 8. Comparison of the channel geometry of the CR and steel die at P2.

In summary, the comparison between the CR and steel dies demonstrates a higher geometric conformity to the CAD geometry for the steel die. The observed deviations of the CR die can largely be attributed to process-related limitations of resin-based additive manufacturing, including limited resolution, light scattering caused by ceramic fillers, and additional smoothing effects during UV post-curing, which particularly affect edge sharpness and fine channel geometries. The remaining deviations of the steel die from the CAD geometry, such as unevenness and variations in channel depth, are mainly associated with a previously identified manufacturing inaccuracy of approximately 0.1 mm.are attributed to a previously noted inaccuracy of about 0.1 mm in the additive manufacturing at IPEG.

The sheet metal blanks were successfully formed without cracking in the first test series. The pure pressing time was 4–5 s; however, additional time had to be considered within the overall cycle for loading and unloading the components. Consequently, the total cycle time from one experiment to the next was approximately 20 s. Fig. 9 shows a representative MPP manufactured with a steel die. The previously defined measurement points P1 to P4 and the derived 2D height profile along the marked measurement path (blue arrow) are shown. From the 2D height profile, it can be seen that channel depths between 0.219 and 0.374 mm were achieved. The highest values were measured in the wider channels P1 and P4. The narrow channels P2 and P3 show a difference of 0.110 mm (P2) and 0.155 mm (P3) compared to the highest channel depth of P1, which is about 30 to 42 % lower than the maximum drawing depth achieved by P1.

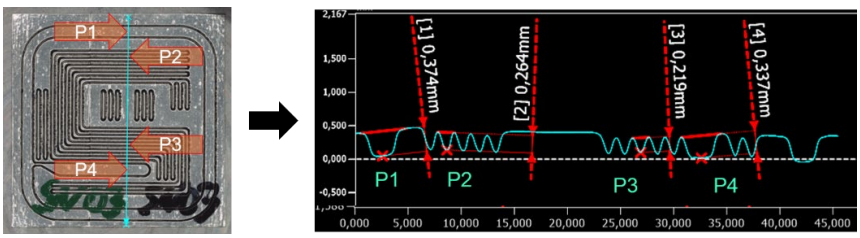

Sheet 2D height profile

Fig. 9. Representative formed MPP with measurement points and extracted 2D height profile.

Fig. 10 shows an exemplary comparison of the actual and target geometries of MPPs manufactured with CR and steel dies. This is a detailed view from the area of the MPP marked on the right. Qualitatively, it can be observed that the channel geometries of the sheets formed with the CR die are closer to the respective target geometry of the die. However, the achieved drawing depths with the steel die are correspondingly higher, and the channel geometry more closely matches the overarching target geometry (reference geometry) that was established as the target dimension before the fabrication of the dies.

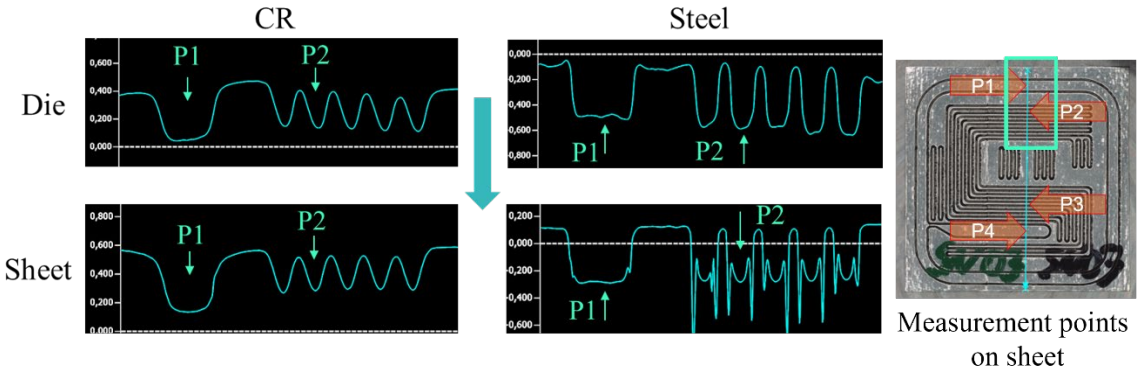

Fig. 10. Comparison of die geometry and component geometry for the (l.) CR and (r.) steel dies.

For a qualitative comparison of the actual and target geometry of the MPP and the die, Fig. 11 presents the evaluation of the determined drawing depths in relation to the target drawing depth of the respective dies (CR and steel) graphically using a boxplot diagram. As shown in Fig. 11, MPPs manufactured with CR dies achieve higher relative drawing depths relative to the die geometry compared to components made with steel dies. In some cases, the achieved channel depths exceeded 100 %. Overall, MPPs produced with the steel die show higher absolute drawing depths than those made with CR. However, except for measurement point P1 (> 90 %), these are significantly below the target depth, ranging between 65 % and 83 %. Generally, wider channels achieved higher relative drawing depths and better dimensional accuracy of the entire channel geometry compared to narrow channels (Figs. 10 and 11).

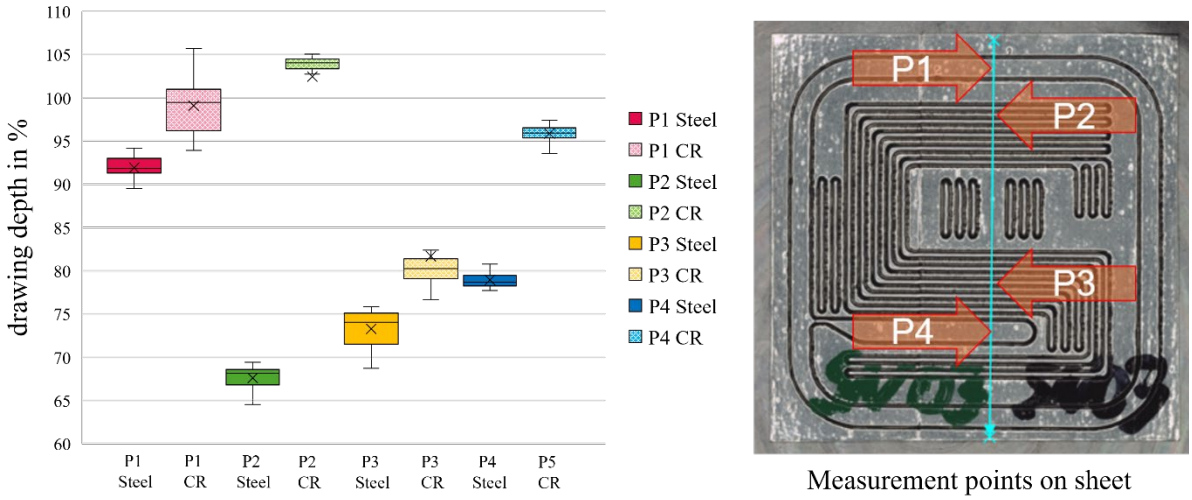

Fig. 11. Comparison of the achieved drawing depths between CR and steel dies for different measurement points.

The overall cycle time of about 20 s (with the exception of failure-related trials involving increased removal times due to required tool disassembly) is primarily determined by tooling and equipment constraints rather than by the forming process itself. Since the actual forming process, defined by the start and end of the press stroke, lasted approximately 4–5 s, a cycle time of less than 7 s appears feasible with optimized equipment, process technology, and automation.

The comparison of the channel depths of the fabricated MPPs reveals a strong dependence on the target geometry of the die and the limitations imposed by the respective manufacturing process. While the CR die shows a higher relative fulfillment of the prescribed channel depth, this is mainly a consequence of its insufficient absolute channel depth and elastic deformation caused by an inhomogeneous modulus of elasticity, which in some cases even results in drawing depths exceeding the die geometry. In contrast, the steel die exhibits lower relative form filling, primarily due to its deeper and sharper channel geometry, which places increased demands on material flow and formability.

Local variations in channel fulfillment are further governed by the spatial position on the MPP and the channel width, as demonstrated by the high degree of filling observed at P1. Enhanced material inflow and more favorable stress conditions in outer regions support forming, whereas narrow channels and sharp edges are adversely affected by the viscoelastic behavior of the rubber, which resists penetration under low holding time and room temperature. To counteract this effect, an increase in holding time was experimentally investigated in order to improve rubber flowability under sustained static pressure. However, longer holding times led to pronounced rubber intrusion into gaps between the die and the draw edge, which prevented non-destructive demolding and caused damage to the components. As a result, this approach could not be further pursued with the current tool configuration. An alternative approach to improve rubber flowability would be tempering the rubber; however, this would significantly increase cycle time and tooling complexity, thereby reducing the economic viability of the process. In addition, the rubber hardness is expected to influence the achievable form filling and channel geometry. This effect was therefore investigated within the parameter study presented in the following section.

The evaluation of the parameter study by creating response surface plots in Minitab shows the influences of rubber hardness, rubber thickness, and pressing force on the achieved drawing depth, as illustrated in Fig. 12 using the example of measuring point P1. The response surface plots each hold one variable constant while relating two others to each other, highlighting the achieved drawing depth. The plots indicate that the greatest drawing depths of approximately 0.397 mm were attained with a rubber thickness of 10 mm. The optimal rubber hardness is 80 Shore A in combination with a pressing force of 300 kN. Additionally, the middle plot shows that the optimal pressing force increases with higher rubber hardness. The smallest drawing depths, below 0.385 mm, were observed with a pressing force of 500 kN in combination with a rubber hardness of 65 Shore A. Both higher and lower rubber hardness than 80 Shore A generally resulted in reduced drawing depths; the same applies for a rubber thickness of 10 mm. The influence of the pressing force depends on the other parameters. With exceptions, the smallest drawing depths occur at a pressing force of 500 kN. Overall, the influence of the varied process parameters on the drawing depth remained limited to a range of 6 to 13 µm.

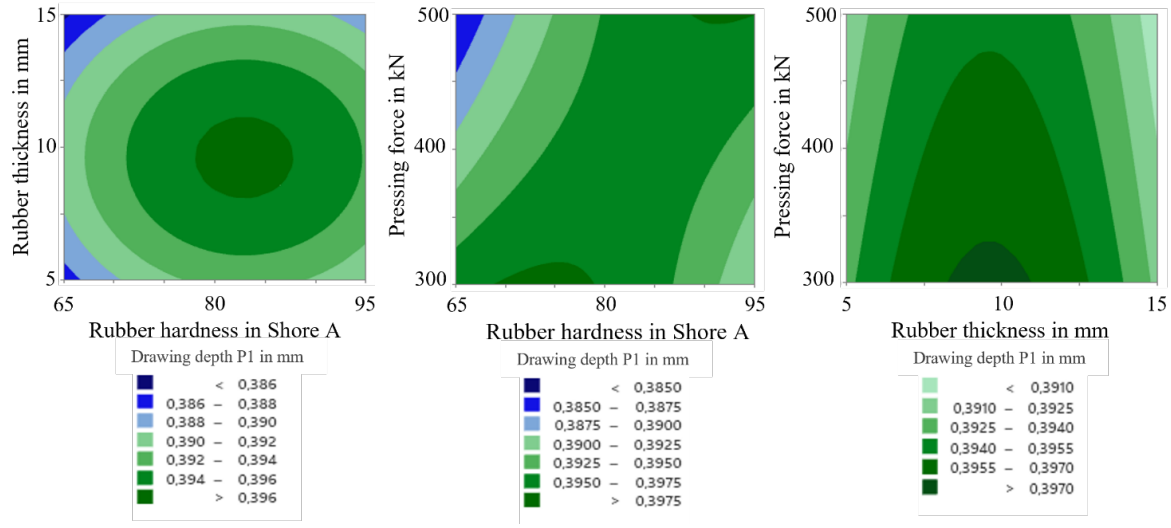

Fig. 12. Influence of pressing force, rubber hardness, and rubber thickness on the drawing depth.

In contrast to the expectations promising a better forming quality with lower rubber hardness, observations showed that the best results were achieved at a Shore A hardness of 80. This is similar to the issue with increased holding time. Softer rubber also increases the risk of jamming and tends to flow into undesirable areas, which can negatively affect component quality as the rubber tends to displace its volume into all cavities, serving only a small portion of the die filling. At the same time, rubber with higher hardness, such as 90 Shore A, would also be disadvantageous, as it offers greater resistance to deformation. This explains the observed dependence of pressing force on rubber hardness: The higher the rubber hardness, the greater the pressing force required to achieve similar drawing depths (see Fig. 12, center). For ongoing investigations, considering effort, feasibility, and especially the scalability of the resulting surface pressure, a rubber hardness of 80 Shore A, a rubber thickness of 10 mm, and a pressing force of 300 kN were selected as suitable. Nevertheless, it should be noted that in the entire parameter study, the range of maximum 13 µm is very limited, which reduces the sensitivity of the measurement values to the parameters. Therefore, further influencing factors and challenges of the currently developed process are addressed in subsequent sections.

In summary, the successful formation of sheet metal blanks without cracking suggests that the chosen process parameters were generally effective. However, the comparison of channel geometries between CR and steel dies reveals important distinctions in their performance and influence on forming behavior.

For the investigation of component warping, forming tests were conducted with a steel die using constant rubber and process parameters, and the results were analyzed as described below. The investigations typically showed a rise in the component center compared to the outer areas. Fig. 13 exemplarily illustrates such a measurement, where the reference lines described in the methodology are shown. A resulting 2D height profile is depicted on the right side and shows a central elevation of 0.248 mm based on the BL-TR line.

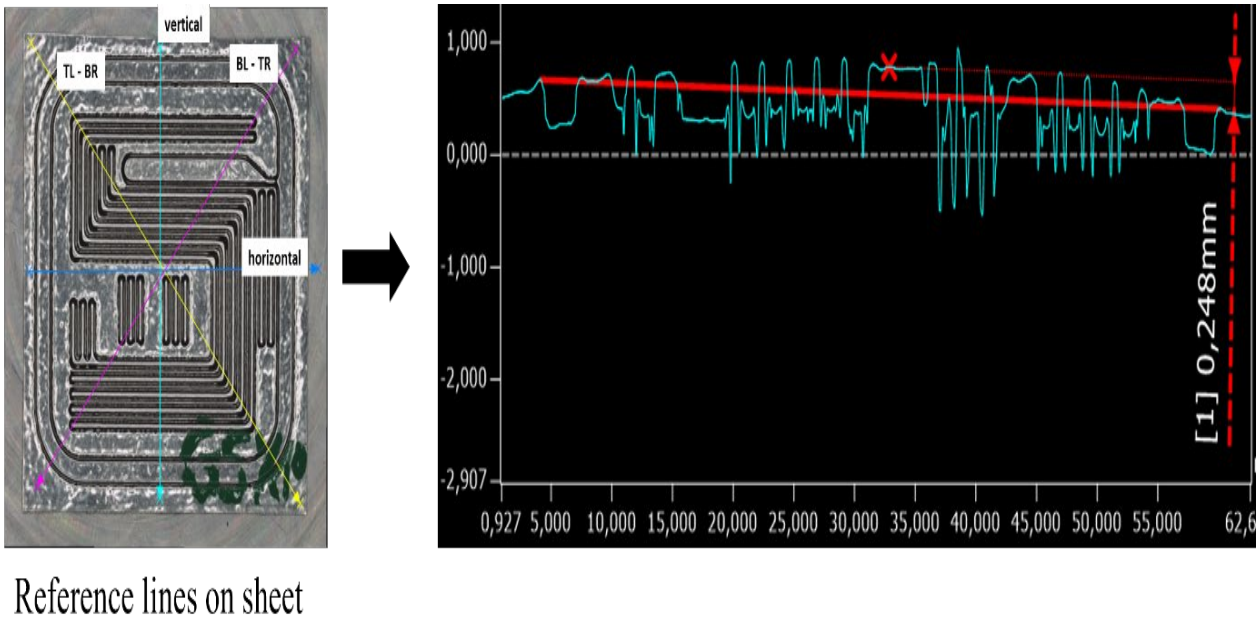

Fig. 13. Optical analysis for determining component warpage.

Fig. 14 shows a representative 3D height profile used for a comprehensive examination of component warping. From the perspective depicted, the central elevation of the component compared to its corner points is evident. The component exhibits asymmetric behavior across its entire surface, as can be seen in the edge areas of the 3D profile in Fig, 14. Moreover, it becomes clear that the degree of warping intensifies disproportionately towards the outer and corner areas.

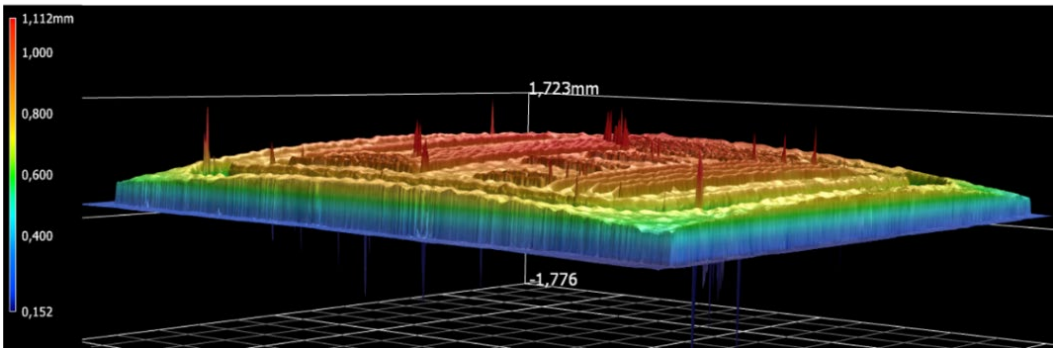

Fig. 14. Representative 3D height map for evaluating component warpage.

The inhomogeneous warping behavior of the components indicates non-uniform stress states in the sheet metal during and after forming, which can mainly be attributed to the asymmetric channel geometry and the resulting uneven stress distribution. Local differences in deformation lead to varying springback behavior and should therefore be considered in future adjustments of the mask geometry. The pronounced deformation observed in corner regions is likely related to the absence of beading structures, which reduces local stiffness and resistance to elastic deformation compared to reinforced areas, thereby promoting increased springback. In addition, these effects may be intensified by an earlier transition to plastic deformation in certain regions or by deformation and partial failure of the rubber, as evidenced by damage observed in the rubber in corner areas after several forming cycles.

Fig. 15 presents an overview of the results related to component warping. In addition to the measurements of the target geometry (Target Steel), it compares the measurement values from the reference experiment with rubber pads (RP) and the various modifications of the experimental setup across all four considered measurement areas. Based on the figure, it is apparent that except for a few exceptions with RV 2mm, all experiments show positive values, indicating an elevation of the component center compared to the outer areas. In contrast, the target geometry displays exclusively negative values between 0,02 and -0.13 mm. The measurement values from all experiments range from approximately -0.29 to 0.52 mm. The test series RSX 2mm and RV 2mm exhibit high variability compared to the other measurements, with a standard deviation of up to 0.179 mm (RV 2mm, vertical). The figure clearly shows that the diagonal TL – BR has the highest values, suggesting that component warping is most pronounced along this line. The lowest values most frequently occur in the horizontal measurement, followed by the vertical measurement. These two measurement areas also show relatively small variations between the different parameters, within a range between 0.08 and 0.18 mm, apart from RSX 2mm and RV 2 mm. The progression of values along the vertical line shows no clear trend, while on the horizontal line a slight decrease is observed from the pure rubber pad to the convex elevation via the steel mask, where the value tends to decrease with increasing mask height. With the increase of the concave steel mask, the horizontal value increases slightly. Apart from outliers, the lowest value of 0.075 mm is observed in the diagonal BL – TR of the RSX 3mm test series. As can be seen in Fig. 15, all measurement areas, except for the diagonal TL - BR, show relatively low values. In the RV 2mm measurement, when including outliers, the lowest values are seen by far, including negative areas, with the lowest value being -0.285 mm and the mean of the measurement series at -0.065 mm. Comparing the RX 2mm and RV 2mm measurements, it is evident that the concavely milled rubber pad leads to predominantly less component warping, although the significance is limited due to the high measurement variability in RV 2mm. Another notable observation is the progression of warping values along the two diagonals, starting with the standard rubber pad through to the combination with the convex and particularly the concave steel mask (GSV) with mask thicknesses of 1, 2, and 3 mm: Except for the RSX 3mm measurement, the warping intensifies in the OL–UR direction with increasing mask height, while it decreases in the UL–OR direction. It can be observed that the values of the two diagonals consistently exhibit an inverse relationship, reflected in a symmetrical progression of measurements parallel to the x-axis at y = 0.25 mm.

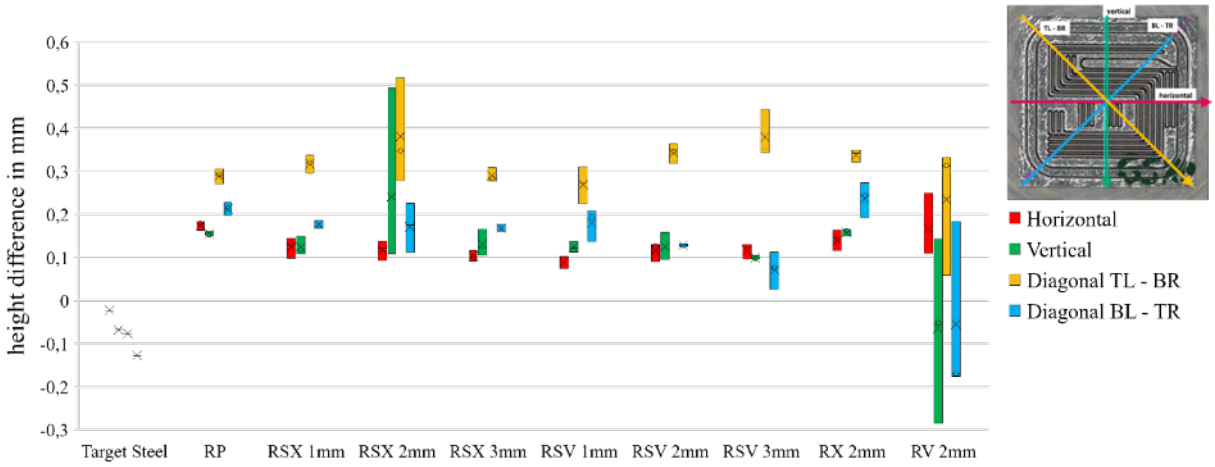

Fig. 15. Influence analysis of convex (RSX) and concave (RSV) steel masks at heights 1, 2, 3 mm, and milled rubber pads with 2 mm elevation (RX) or recess (RV) on warpage compared to target geometry of steel die (Target Steel) and standard rubber pad reference (RP).

Deviations between vertical, horizontal, and diagonal warping measurements can partly be explained by geometric effects described by the intercept theorem, which predicts more pronounced bending along diagonal directions for identical curvature radii. This behavior further suggests an increased stress gradient between the component center and edge regions along the diagonals, particularly towards the corners. This assumption is confirmed by the three-dimensional component geometry analysis and is consistent with the previously discussed interpretations.

Despite partly ambiguous trends associated with convex and concave tool modifications, distinct correlations are observed. Horizontal warping decreases with increasing convex steel mask height and increases with increasing concave mask height, indicating a clear influence of stress redistribution induced by tool geometry. These findings support the assumption that a time-dependent redistribution of stresses significantly affects forming behavior and final component flatness. Notably, negative warping values observed in parts of the RV 2 mm test series, where the component center exhibits downward deformation, warrant further investigation to assess measurement reproducibility and to derive targeted measures for reducing warping. Reproducibility is therefore identified as a key prerequisite for reliably evaluating parameter-dependent trends.

An additional relevant observation is the inverse relationship between different measurement areas, particularly between the two diagonal height profiles. This suggests that warping induced by the mask geometry in one diagonal direction can partially compensate for warping in the orthogonal diagonal. The mechanical origin of this behavior lies in the targeted modification of the pressure distribution by the steel masks, which can geometrically direct warping into preferred directions. As a result, one diagonal exhibits increased warping while the orthogonal diagonal shows reduced deformation. This effect may offer advantages during component assembly and has the potential to mitigate snap-through behavior, which depends on the existing residual stress state. The influence of mask geometry on local stress and strain distributions during forming thus directly explains the observed changes in the height profiles and will be further investigated in subsequent work packages.

Conclusion

This study investigated the potential of the rubber drawing process for the production of metallic MPPs for use in PEMFCs. The focus was on dimensional and form accuracy in relation to process parameters such as pressing force, holding time, rubber hardness, rubber thickness, and the influence of concavely and convexly modified rubber pads. Additionally, the quality and suitability of additively manufactured CR and steel dies were analyzed.

The investigation of the additively manufactured dies revealed that dies made from CR were not suitable for use due to an insufficient and inhomogeneous modulus of elasticity. Furthermore, the

CAD geometry could not be precisely realized with these materials, which further restricted the quality of the MPPs produced with them. In contrast, steel dies showed higher precision and less distortion during fabrication, making them more suitable for use, although there is still potential for optimization in manufacturing accuracy.

The experimental investigations demonstrated the potential of the rubber pad forming process to offer economic advantages over the competing hydroforming process, particularly in terms of reduced equipment and tooling costs as well as potentially shorter cycle times. However, the major challenge remains the reliable fulfillment of the geometric requirements of the manufactured components. The examination of rubber and process parameters demonstrated that targeted adjustments, particularly of rubber materials in terms of hardness and thickness, achieved improvements in the dimensional accuracy of the MPPs. A Shore A hardness of 80, in combination with a thickness of 10 mm and a pressing force of 300 kN, was identified as optimal, as this parameter set provides a balanced compromise between sufficient stiffness and adequate flowability of the rubber. This configuration allowed for the best possible dimensional accuracy, with values of nearly 95% of the tool's specified target value being reached for the wide outer channels, which can be attributed to improved material inflow and more favorable stress conditions in these regions, while measurement sensitivity ranged from 6 to 13 µm. The analysis also highlighted that both the hardness and viscoelastic properties of the rubber are critical factors for dimensional accuracy, since they directly govern elastic deformation, flow resistance, and local form filling. Lower Shore A hardness and extended holding times improve flow capacity, particularly in deeper or sharper channel geometries, but simultaneously increase the risk of jamming and undesirable flowing into cavities, caused by excessive elastic deformation and uncontrolled material migration, negatively impacting component quality.

Another significant finding was achieved through the modification of rubber pads and the associated shift in stress distribution. The use of concavely and convexly modified rubber pads enabled the targeted manipulation of local pressure distribution. This led to a reduction in component warping in certain areas of the plate structure. In some cases, these effects were offset by increases in other directions, indicating an inverse relationship, for example, between warping values along different diagonals. This effect could help direct component warping in a specific direction, reduce local stresses, and thus improve the overall stability of the MPPs. This could also minimize the 'snap-through' effect, which is associated with residual stresses in the components.

Overall, the study demonstrates the potential of the rubber drawing process for the production of MPPs, but it also emphasizes that further optimizations in material selection, tool geometry, and process control are necessary. These adjustments are critical to further improve dimensional accuracy, process stability, and reproducibility, and to promote the economical use of the process in large-scale applications.

Outlook

The current investigations have shown that optimizing process conditions can significantly improve the component quality in the production of metallic MPPs. In particular, the results suggest that precise control of process parameters such as Shore hardness, pressing force, holding time, and mask geometry is essential for achieving more accurate form filling and improved dimensional accuracy, as these parameters collectively govern the viscoelastic deformation, flow resistance, and elastic recovery of the rubber, which in turn determine local material inflow and geometric fidelity during forming.

However, the use of high-precision techniques, such as CNC micro-milling or more precise 3D printing for die manufacturing, could further enhance the control over component geometries. Simultaneously, more modern presses and the implementation of an optimized rubber housing design could facilitate longer holding times without causing blockages.

Moreover, a key approach lies in further developing die and channel geometries. Targeted recesses or undercuts can help compensate for the springback effect of stainless steel. Additionally, concave and convex mask geometries could be advanced to ensure even stress distribution and prevent uneven component deformation.

Additional approaches include the use of lubricants, such as spray water, to minimize friction between rubber and sheet metal as well as tool wear. Furthermore, simulation-based approaches employing hyperelastic material models could enable more precise process control by better accounting for complex material properties.

Looking ahead, the current research project envisages the production of milled dies and the adjustment of die geometries to effectively reduce component warping. Additionally, the project plans to determine the wear limits of different rubber variants through fatigue tests.

Combining these measures could not only significantly optimize the quality and efficiency of MPP manufacturing but also support their application in sustainable mobility.

Acknowledgement

This research project was carried out as a cooperative project between companies (Aspens) and research institutions (IFUM) within the Central Innovation Programme for small and medium-sized enterprises (ZIM). ZIM is a funding programme of the Federal Ministry for Economic Affairs and Energy. The project was supervised and administered by AiF Projekt GmbH, acting in a fiduciary role. We would like to express our special thanks to Aspens GmbH, the project partner, for their willingness to cooperate, as well as for providing the necessary materials and their comprehensive expertise.

References

[1] A. Hermann, T. Chaudhuri, P. Spagnol, Bipolar plates for PEM fuel cells: A review, Int. J. Hydrogen Energy 30 (2005) 1297-1302.

[2] ASM International, ASM Handbook, Volume 14: Forming and Forging, ninth ed., American Society for Metals, 1988.

[3] X. Li, Proton exchange membrane fuel cells: Principles, technologies and applications, Energy Rep. 10 (2024) 112-135.

[4] J. Wind, R. Späh, W. Kaiser, G. Böhm, Metallic bipolar plates for PEM fuel cells, J. Power Sources 105 (2002) 256-260.

[5] H. Kahraman, Y. Çevik, A review of bipolar plates for proton exchange membrane fuel cells, Int. J. Energy Res. 35 (2011) 558-570.

[6] C. Bauer, A. Schröder, J. Reimer, Manufacturing technologies for metallic bipolar plates: A review, J. Manuf. Process. 45 (2019) 367-381.

[7] J. Mueller, J. Dawson, A. Radtke, Hydroforming of thin metallic sheets for PEM fuel cell bipolar plates, Procedia Manuf. 12 (2016) 375-382.

[8] J. Dawson, M. Walker, Continuous embossing of metallic bipolar plates for PEM fuel cells, Int. J. Hydrogen Energy 40 (2015) 11773-11781.

[9] W. Lee, S. Kwon, Y. Kim, High-speed embossing process for PEM fuel cell bipolar plates, J. Mater. Process. Technol. 140 (2003) 70-76.

[10] P. Groche et al., Sheet metal forming using elastomer tools – State of the art and future trends, CIRP Ann. 63 (2014) 683-705.

[11] A. Abedian, F. Pourboghrat, Analysis of the rubber-pad forming process, J. Mater. Process. Technol. 100 (2000) 10-16.

[12] J. Kim, H. Kim, Optimization of rubber pad forming for sheet metals with complex surface patterns, Met. Mater. Int. 24 (2018) 321-330.

[13] M. Elyasi, H. Talebi Ghadikolaee, M. Hosseinzadeh, Fabrication of metallic bipolar plates in PEM fuel cell using semi-stamp rubber forming process, Int. J. Adv. Manuf. Technol. 92 (2017) 765-776.

[14] S. Hashemi, A. Roohi, Fabrication of aluminum bipolar plates with Archimedes' screw-shaped channels: A rubber pad forming process assessment, SN Appl. Sci. 3 (2021) 909.

[15] M. Elyasi, F.A. Khatir, M. Hosseinzadeh, Investigation of die clearance in rubber pad forming of metallic bipolar plates, Mech. Eng. J. 1 (2016) 89-98.

[16] N. Albers, A. Ngondji, Experimental evaluation of a feature-based bipolar plate forming approach in a hybrid tool, MATEC Web Conf. (2025).

[17] P. Groche, A. Huttel, C. Müller, Analysis of the rubber pad forming process with respect to material flow and pressure distribution, J. Mater. Process. Technol. 214 (2014) 1853-1864.

[18] Y. Kim, S. Kim, Study on the forming behavior of metal foils in rubber pad forming process, Int. J. Precis. Eng. Manuf. 19 (2018) 375-384.

[19] A. Kampker, H. Heimes, Elektromobilität, Springer Verlag, 2024.

[20] Graebener Maschinentechnik GmbH & Co. KG, Information on https://www.graebener.com/de/formen.

The publication of this article was funded by the Leibniz Universität Hannover (LUH) / Technische Informationsbibliothek (TIB)